Nano Research

Open Access

Research Article

Orchestrating nanocrystal orientation in dynamic networks: A low-loading strategy for high-performance bio-photonic films

Yiwen Ren[1,§], Lina Meng[1,§], Qianwen Luo[2], Adnan Raza Altaf[1], Tengwen Lin[1], Qun Song[3], Luogen Peng[4], Shuiping Yan[1], Jing Liu[1], Dingding Yao[1], and Peiwen Liu[1]✉

[1] *College of Engineering, Huazhong Agricultural University, Wuhan 430070, China*
[2] *College of Water Resources and Hydropower Engineering, Wuhan University, Wuhan 430072, China*
[3] *Sustainable Materials and Chemistry, Department of Wood Technology and Wood-based Composites, University of Göttingen, Büsgenweg 4, D-37077 Göttingen, Germany*
[4] *Department of Oncology, Changsha Central Hospital, University of South China, Changsha 410004, China*
§ *Yiwen Ren and Lina Meng contributed equally to this work.*

Cite this article: *Nano Research*, **2026**, *19*, 94908338. https://doi.org/10.26599/NR.2026.94908338

ABSTRACT: The bond dissociation–recombination behavior of dynamically crosslinked networks provides a fundamental physical mechanism underlying the ordered alignment of nanomaterials. This study employs dynamic covalent hydrogels as a model system to systematically elucidate the precise regulation mechanism of cellulose nanocrystal (CNCs) alignment under uniaxial stretching. Results revealed that the rapid recombination of reversible bonds facilitates the effective dissipation of localized stress and serves as "molecular-level bearings", which guide the coordinated rotation and long-range alignment of CNCs along the stretching direction. Besides, under optimized conditions, the resulting composite material exhibits a birefringence of 0.00461 and an orientation index of 0.90754, indicating pronounced optical anisotropy. Through mechanistic understanding, we established a comprehensive processing–structure–property relationship by correlating key parameters (precursor composition, stretching conditions, and geometric dimensions) with the resulting microscopic orientation and macroscopic optical performance. This investigation establishes a foundation for identifying the critical processing window required for developing high-performance, low-cost, and sustainable photonic materials.

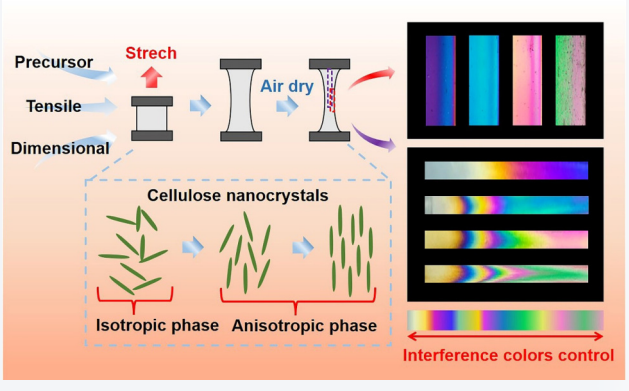

KEYWORDS: dynamic covalent networks, cellulose nanocrystals alignment, optical anisotropy, photonic materials, bond dissociation–recombination

1 Introduction

Cellulose nanocrystals (CNCs) are one-dimensional rod-like nanomaterials, derived from natural cellulose emerged as a focal point in advanced material research owing to their abundance and exceptional biocompatibility with outstanding mechanical properties [1]. Structurally, CNCs exhibit a high aspect ratio and large specific surface area [2], possess abundant chemically modifiable surface functional groups [3], and demonstrate a high elastic modulus arising from their rigid rod-like architecture. These attributes render CNCs an ideal nano-reinforcing phase, capable of serving as a "bridge" that transfers nanoscale properties to the macroscopic level, thereby enabling the structural order and enhancing the material performance. Notably, the ability to lock the nanoscale ordered structure of CNCs enables the fabrication of macroscopic materials with photonic bandgaps and structural colors [4], highlighting their significant potential in applications such as photonic pigments [5], optical sensors [6], and anti-counterfeiting technologies [7].

However, bridging the gap between nanoscale order in CNCs and high performance in macroscopic materials remains a significant challenge in fabrication science. Evaporation-induced self-assembly (EISA) remains a classical approach for fabricating CNCs-based photonic crystals; however, this process is highly time-

Received: November 29, 2025
Accepted: December 8, 2025

✉Address correspondence to peiwenliu@mail.hzau.edu.cn

consuming, often requiring several days to weeks [8], and is critically dependent on stable environmental conditions such as temperature and humidity [9]. Even minor environmental fluctuations can readily induce structural defects (e.g., cracks and multi-domain orientations) [10], resulting in non-uniform optical properties that significantly hinder practical applications and scalable production. To overcome the inherent limitations of EISA process, various strategies have been developed to induce alignment through external fields. Although shear flow fields are operationally simple, the induced alignment is often restricted to the surface or near-surface regions of the material, making it challenging to achieve uniform bulk alignment [11]. In contrast, the electric or magnetic field induction provides an improved spatial control, although these methods generally require expensive precision equipment and specially designed molds, which can compromise the process simplicity and cost-effectiveness [12]. In this context, the stretch-induced alignment emerged as a direct and efficient mechanical approach for achieving molecular orientation. By applying uniaxial stretching to polymer films or gels containing CNCs, this approach compels the embedded nanocrystals to reorient along the stretching direction, thereby significantly enhancing the overall degree of alignment within the resulting solid composites [13].

Hydrogels are soft materials characterized by hydrophilic three-dimensional network structures, and are commonly used as matrices for CNCs composites [14]. The nature of the crosslinks within these networks fundamentally determines the macroscopic mechanical behavior and structural reconfigurability of the materials. These crosslinks can be broadly classified into two categories: irreversible crosslinks-primarily permanent covalent bonds that form stable networks [15] and reversible crosslinks, which include dynamic covalent bonds (e.g., imine bonds and Diels–Alder reactions) as well as physical interactions such as hydrogen bonding, ionic coordination, and host–guest recognition, all of which impart dynamic and adaptive characteristics to the network [16].

To date, studies have merely demonstrated that applying shear to hydrogel matrices can induce directional alignment of CNCs, and the resulting ordered structure critically determines the final properties of the composites [13]. To our knowledge, studies have not been conducted or limited to investigate the shear fields, which are the key factors for orchestrating the CNCs features in a dynamic system. For the first time, in this work we focused on shear fields for understanding the systematic alignment capability of uniaxial stretching enacted to achieve uniform bulk orientation within hydrogel system under different crosslinking classes, such as irreversible and reversible types. Besides, we further investigated how precursor parameters (e.g., crosslinking density and polymer concentration) and stretching parameters (e.g., strain rate and elongation ratio) synergistically govern the final oriented structure and alignment kinetics of CNCs.

Through comparative analysis, we elucidated the unique advantages and underlying physical mechanisms of reversible dynamically crosslinked networks in promoting efficient and uniform CNCs alignment. Moreover, by optimizing processing parameters, the raw material consumption is substantially reduced, and the resource utilization efficiency is significantly enhanced, thereby offering a new paradigm for green and sustainable manufacturing for next-generation ultra-low-power reflective displays and adaptive optical devices.

2 Experimental

2.1 Materials

CNCs were purchased from ScienceK. 2,2,6,6-Tetramethylpiperidin-1-oxyl (TEMPO), 3-(acrylamido) phenylboronic acid (PBAAM), methacrylic anhydride, 2,4,6-trimethylbenzoyl chloride, lithium bromide, acrylamide (AM), sodium sulfate anhydrous, sodium tetraborate decahydrate, N,N′-methylenebisacrylamide (MBA), 4,4′-azobis (4-cyanovaleric acid) (ABCV), polyvinyl alcohol (PVA), sodium bicarbonate, tetrahydrofuran (THF), ethyl acetate, and n-hexane were purchased from Macklin. Dopamine hydrochloride and dimethyl phenylphosphonite were obtained from Aladdin. Microcrystalline cellulose (MCC), hydrochloric acid, and butan-2-one were ordered from Shanghai Hushi. Deionized water used in all experiments was purified using an ultrapure water system. Dopamine methacrylamide (DMA) and lithium phenyl-2,4,6-trimethylbenzoylphosphinate (LAP) were synthesized according to the established methods (Figs. S1–S4 in the Electronic Supplementary Material (ESM)).

2.2 Synthesis of purely covalently crosslinked hydrogels

Purely covalently crosslinked hydrogels were prepared following a reported method [17]. AM was used as the monomer, MBA as the crosslinker, and ABCV as the radical initiator. In the hydrogel precursor, the concentration of AM was 2 wt.%; CNCs concentrations were 0 wt.% and 2 wt.%, respectively; the contents of MBA and ABCV were 0.02 mol% and 0.25 mol% relative to AM, respectively. The precursor was repeatedly purged with nitrogen gas before being poured into a rectangular mold. Gelation was carried out for 6 h at 40 °C under a N_2 atmosphere. The resulting gels were then cooled to room temperature to obtain the purely covalently crosslinked hydrogels.

2.3 Synthesis of purely hydrogen-bonded hydrogels

20 g of PVA was dissolved in 80 g of water by allowing it to swell at room temperature for 1 h, followed by heating and stirring at 90 °C for 2 h to form a homogeneous transparent solution. A high-concentration CNCs suspension was added to dilute the PVA in the precursor solution to 10%, with the final CNCs concentrations being 0 wt.% and 2 wt.%. The precursor solution was poured into a clean culture dish and subjected to cyclic freeze-thawing: freezing at −18 °C for 21 h followed by thawing for 3 h. This freeze-thaw cycle was repeated three times to obtain the physically crosslinked hydrogels.

2.4 Preparation of dynamic covalently crosslinked hydrogels

Dynamic hydrogels were prepared according to a reported method [13]. Polyvinyl chloride films were used as spacers to control the hydrogel thickness. CNCs suspensions were incorporated into the hydrogel precursor solution. The precursor mixture consisted of a borax-sodium hydroxide buffer (pH = 10, 0.0125 M), AM (2 M) as the monomer, DMA/PBAAM (synthesized to constitute x mol% (x = 1.25) of the total acrylamide) as the crosslinker, and LAP (0.5 wt.%) as the photoinitiator. The final buffer concentration in the hydrogel precursor was 0.0125 M. The precursor was purged with N_2 for 3 min to remove dissolved oxygen and then exposed to ultraviolet (UV) light (wavelength of 300–400 nm, 8 W) for 30 min to complete the gelation process. Unless otherwise specified, the

CNCs suspension was incorporated into the hydrogel precursor solution at a ratio of 2 wt.%.

2.5 Fabrication of CNCs-composite photonic gel materials

Uniaxial stretching was employed to fabricate the photonic gel materials. The uniaxial stretching of the hydrogels was performed using a microcomputer-controlled electronic universal testing machine. Tensile tests on freshly prepared hydrogels were conducted at 25 °C and 35% relative humidity. The default dimensions of the hydrogels for tensile tests were 10 mm in width, 2 mm in thickness, and 8 mm in length. The tensile speed for uniaxial stretching was set at 2.5 mm/min. Stretching was stopped upon reaching an elongation ratio (λ) of 6. The stretched state was maintained, and the samples were allowed to dry naturally on the tensile testing machine until a constant weight was achieved.

2.6 Characterization methods

^{1}H solid-state nuclear magnetic resonance (^{1}H NMR) spectroscopy: The synthesized solid sample was placed in a clean, dry NMR tube and fully dissolved using an appropriate solvent. Measurements were performed on a fully digital superconducting NMR spectrometer (Avance 3600 MHz). Deuterated dimethyl sulfoxide (DMSO-d_6) and deuterium oxide (D_2O) were used as solvents, with residual solvent peaks referenced at δ = 2.50 and 4.79 ppm, respectively.

Transmission electron microscopy (TEM): A cellulose nanocrystal suspension was prepared in ultrapure water at a concentration of 0.05 wt.% for morphological and dimensional characterization. The sample was stained with a phosphotungstic acid solution (2 wt.% in water, pH adjusted to 7.0 using 1 M NaOH). TEM observations were conducted using an HT7800 transmission electron microscope (Hitachi) operating at an acceleration voltage of 120 kV.

Mechanical testing: Tensile tests were performed using a UTM2000 electronic universal testing machine (Sansi Zongheng Technology Co., Ltd., Shenzhen). A load cell with a rated capacity of 100 N was used. All tests were conducted at an ambient temperature of 25 °C and a relative humidity of 35%.

Two-dimensional wide-angle X-ray scattering (2D-WAXS): 2D-WAXS measurements on xerogels were conducted using a Xeuss 2.0 instrument (Xenocs, France) equipped with a Cu Kα X-ray source (wavelength λ = 1.54189 Å) operating at 30 W. A Pilatus 3R 300K detector with a pixel size of 172 μm was used. The orientation of the CNCs within the xerogels was quantified using the azimuthal intensity distribution profile along the arc corresponding to the (200) reflection of cellulose Iβ crystals. The orientation index (f) was calculated from the intensity distribution profile in the azimuthal angle (ϕ) according to Eq. (1)

$$f = \frac{180° - \text{fwhm}}{180°} \quad (1)$$

where fwhm is the full width of the half-maximum of the azimuthal profiles from the selected equatorial reflection.

Transmittance measurements: Transmittance spectra of the hydrogels across the wavelength range of 200–900 nm were recorded using a V-1300 UV–visible (UV–Vis) spectrophotometer (Macy Instrument Co., Ltd., Shanghai). Sample dimensions for testing were 1 cm × 3 cm.

Cross-polarized optical microscopy (POM): The characterization was performed using a BH200M polarized optical microscope (Ningbo Sunny Instruments Co., Ltd.) equipped with crossed polarizers in reflection mode. The specimens were mounted on glass substrates and characterized under ambient conditions, with the azimuthal angle of the xerogel films along the orientation direction set at 45° to achieve maximum light intensity.

Thickness measurement: The thickness of the xerogel films was measured using an ID-C0512CNXB digital micrometer (Mitutoyo). The instrument was zeroed prior to use, and the probe was carefully positioned at the measurement location. Each measurement was repeated three times to obtain an average value, ensuring data reliability and reproducibility.

Optical retardation: The ratardance measurement of specimens was performed with an LV100-P polarizing microscope from Nikon. The retardation was measured by a Berek compensator and calibrated by the machine constant table.

Birefringence calculation: The birefringence (Δn) was calculated according to Eq. (2)

$$\Delta n = \frac{\Gamma}{d} \quad (2)$$

where Γ is the optical retardation and d is the thickness of the photonic gel film.

Contraction ratio in width: The lateral contraction ratio of the photonic gel film was calculated according to Eq. (3)

$$\text{Contraction ratio in width} = \frac{(W_{\text{initial}} - W_{\text{final}})}{W_{\text{initial}}} \times 100\% \quad (3)$$

where W_{initial} is the initial width of the hydrogel and W_{final} is the final width of the photonic gel film.

3 Results and discussion

3.1 Precursor composition

Three types of hydrogel systems with distinct crosslinking mechanisms were systematically prepared and compared: (1) permanently covalently crosslinked hydrogels, fabricated via acrylamide polymerization using MBA as the crosslinker; (2) physically crosslinked hydrogels based on PVA, formed through cyclic freezing–thawing driven by hydrogen bonding; and (3) dynamic covalently crosslinked hydrogels, synthesized via *in situ* polymerization of acrylamide in an alkaline buffer, employing phenylboronic acid (PBA)/catechol complexes as dynamic crosslinkers.

CNCs were prepared by sulfuric acid hydrolysis, exhibiting a needle-like morphology with an average length of 182.68 ± 28.50 nm and a diameter of approximately 7.50 ± 1.53 nm (Fig. S5 in the ESM). Zeta potential measurements confirmed that the CNCs possessed a negative surface charge (–39.97 ± 3.67 mV), with the large absolute value indicating good colloidal stability and dispersion in aqueous solution.

3.1.1 *Hydrogel types*

Regarding optical properties, both the permanent covalent and dynamic covalent crosslinked hydrogels exhibited high transparency. In contrast, the hydrogen-bonded hydrogel showed drastically reduced transparency due to significant light scattering caused by microcrystalline regions formed from PVA molecular chains during the freeze-thaw process (Fig. 1(a)). Observations under polarized light (Fig. 1(b)) revealed that in the absence of

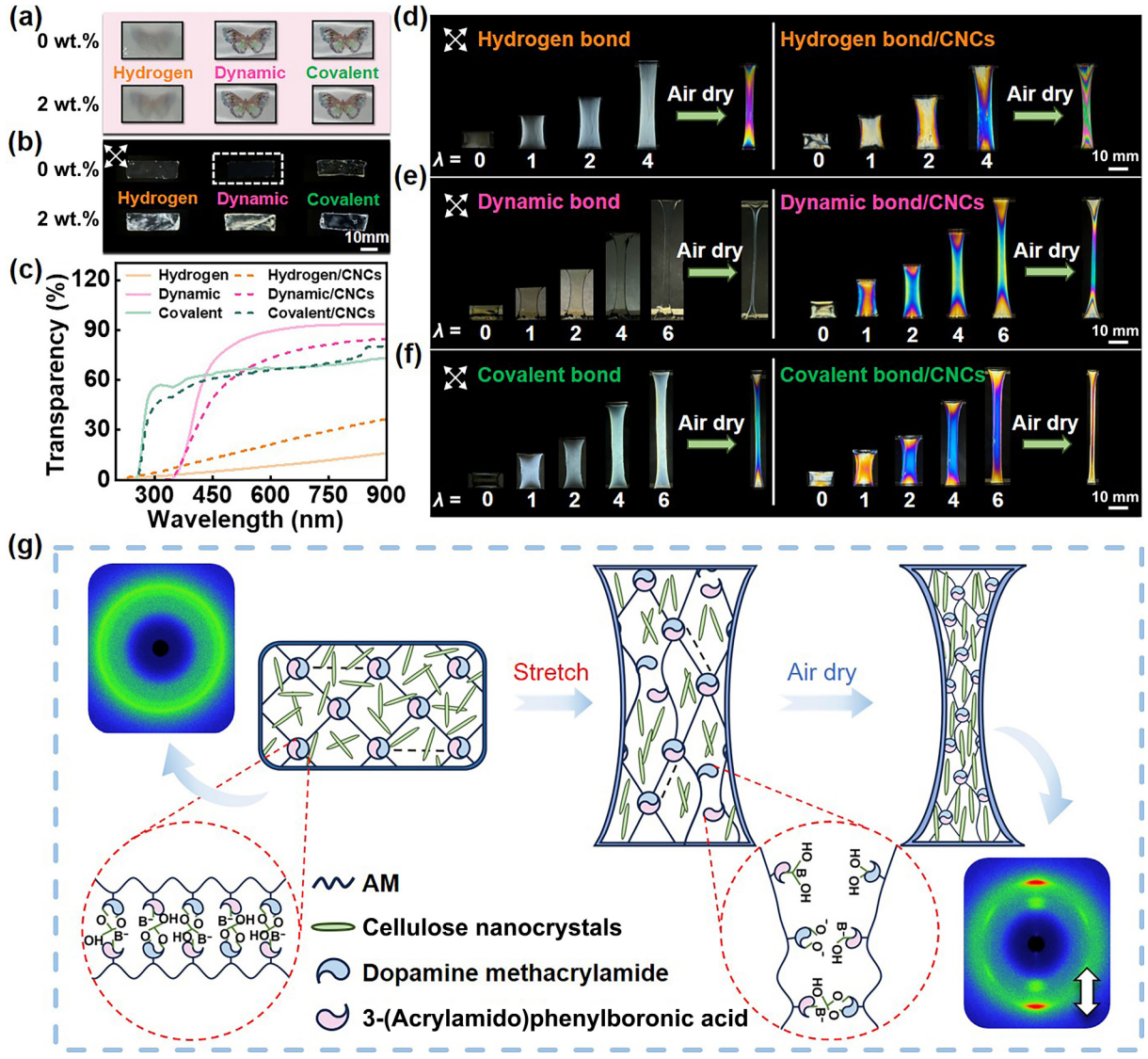

Figure 1 Investigation of the regulatory mechanisms of crosslinking strategies on the optical anisotropy and strain-responsive behavior of hydrogels. (a) Macroscopic morphology of the hydrogels. (b) Polarized optical images showing intrinsic birefringence characteristics. (c) UV–Vis absorption spectra. Polarized optical images of (d) hydrogen-bonded, (e) dynamic covalent, and (f) permanently covalent hydrogels at varying elongation ratios (λ), illustrating the evolution of the orientation structure of CNCs (0 wt.% and 2 wt.%). (g) Schematic illustration of the structural evolution of dynamic covalent hydrogels under uniaxial stretching, with corresponding 2D-WAXS patterns at $\lambda = 0$ and $\lambda = 6$. These results provide direct evidence of the strong preferential alignment of CNCs along the stretching direction.

CNCs, both the hydrogen-bonded and permanent covalent hydrogels displayed only weak birefringence, attributable to local ordering of their polymer chains. The dynamic covalent hydrogel showed no significant birefringence, reflecting its molecular-level isotropy. Upon the incorporation of 2 wt.% CNCs, all three hydrogel types exhibited significantly enhanced birefringence. This transition results from the directional alignment of CNCs, which occurs when their concentration exceeds a critical value, driven by synergistic effects of electrostatic repulsion and steric hindrance that ultimately form liquid crystalline microstructure with long-range order and confer macroscopic optical anisotropy to the composite materials [18, 19].

The quantitative comparison of transmittance in the visible light region further indicated that the dynamic covalent hydrogel possessed the highest transmittance among all samples. In contrast, the crystalline regions formed between PVA and CNCs in the hydrogen-bonded hydrogel acted as light scattering centers, causing reflection, refraction, and scattering of incident light. Particularly when the size of these crystalline regions exceeded the wavelength of incident light, a significant reduction in system transparency occurred [20]. Notably, the incorporation of 2 wt.% CNCs resulted in a slight increase in the transmittance of the hydrogen-bonded hydrogel. This improvement is attributed to the strong hydrogen-bonding network formed between the CNCs and the polyvinyl alcohol chains. This network not only promotes the uniform dispersion of the CNCs but, more critically, disrupts and suppresses the regular arrangement and macroscopic crystallization of the PVA chains. Consequently, the dominant type of light-scattering centers within the system shifts from micrometer-sized crystalline regions to a nano-sized dispersed phase, leading to an overall reduction in light scattering. In the PAM-based hydrogels (including both permanent and dynamic covalent systems), the weaker interaction between amide groups ($-CONH_2$) and CNCs surface hydroxyl groups led to a tendency for CNCs to agglomerate,

forming micron-scale pore structures that enhanced light scattering and reduced transmittance [21]. Furthermore, the analysis of the absorption behavior in the UV region (200–400 nm) revealed that the pure hydrogen-bonded hydrogel and its composite exhibited almost no UV shielding function. In contrast, both PAM-based hydrogels (permanent and dynamic covalent) demonstrated certain UV resistance, with the dynamic covalently crosslinked hydrogel exhibiting the most excellent UV absorption capability (Fig. 1(c)).

The birefringence behavior of the three types of hydrogels during uniaxial stretching (λ = 6) and subsequent air-drying was systematically investigated under polarized light. Both the permanent covalently crosslinked PAM hydrogel and the hydrogen-bonded PVA hydrogel without CNCs exhibited significant interference colors after stretching and drying. This phenomenon is attributed to the stretch-induced reorientation of polymer chains along the force direction, forming optically anisotropic regions, which generates optical retardation and leads to interference (Figs. 1(d) and 1(f) [22]. In contrast, the dynamic covalently crosslinked system exhibited a fluid-like response during stretching due to the continuous breaking and reformation of boronic ester bonds, making it difficult for the polymer chains to maintain long-range ordered alignment, resulting in a significantly reduced birefringence signal. Only during the air-drying process did volume contraction induced by water evaporation promote local alignment of some chain segments, producing weak white-light interference (Fig. 1(e)). Although hydrogen bonds are also reversible, their fast response and high recombination rate enabled the polymer chains to rapidly reconfigure and form an ordered structure under external force, thus exhibiting pronounced birefringence during stretching [23].

Upon the incorporation of CNCs into all three hydrogel systems, significant birefringent colors were observed even at the initial stretching stage, indicating that the introduction of CNCs is the key factor inducing optical anisotropy in the materials at low strain. Further studies revealed that in the permanently covalently crosslinked hydrogel, due to the lack of a dynamic bonding mechanism to maintain the oriented configuration of the CNCs, their alignment gradually relaxed upon the stress release after the stretching ceased, leading to a weakened final order of interference colors (Fig. S6 in the ESM) [24]. In contrast, in reversibly crosslinked hydrogels (hydrogen-bonded and dynamic covalent), the reorganization–reconstruction mechanism of dynamic bonds and their relaxation time difference with CNCs can effectively preserve the CNCs alignment formed during stretching [13]. Subsequently, during air-drying, the contraction of the polymer network further restricted the mobility of the CNCs, promoting an increase in the order of the interference colors.

Mechanical property testing results further corroborate the described behavioral differences (Fig. S7 in the ESM). The covalently crosslinked hydrogel exhibited high strength, high modulus, and low extensibility, fracturing rapidly after yielding characteristics indicative of typical brittle failure and high rigidity. In contrast, the dynamic covalently crosslinked hydrogel demonstrated exceptional ductility enabled by the reversible breakage–recombination mechanism of boronic ester bonds. However, continuous stretching-induced bond exchange reactions led to a loss of mechanical memory, resulting in a gradual decay of load-bearing stress with increasing elongation [25]. Although the hydrogen-bonded system showed weaker overall mechanical properties, its stress–strain curve exhibited no decline with increasing elongation, benefiting from the rapid breaking and reforming kinetics of hydrogen bonds.

It is noteworthy that although the CNCs incorporation introduces hydrogen-bonding interactions in both permanent and dynamic covalent systems, their ultimate effect on CNCs alignment is governed by the nature of the crosslinked network. In permanent covalent networks, the dominant entropic elastic recovery overwhelms the stabilizing role of hydrogen bonds, leading to the relaxation of CNCs orientation. Conversely, in dynamic covalent networks, the stress dissipation mechanism eliminates the elastic retraction drive, allowing hydrogen bonds to synergize with dynamic covalent bonds to effectively guide and lock the stretch-induced alignment of CNCs.

Furthermore, the incorporation of CNCs significantly enhanced the elastic modulus and ultimate strength of all three hydrogel types. This confirms that CNCs serve not only as functional components for optical tuning but also as highly efficient multifunctional nano-reinforcing phases capable of synergistically improving the comprehensive mechanical performance of hydrogels [26].

To gain deeper insight into the alignment evolution mechanism of CNCs within the dynamic covalently crosslinked hydrogel during uniaxial stretching, this study combined 2D-WAXS characterization and structural modeling to systematically elucidate the microstructural reorganization pathway and the origin of optical anisotropy. 2D-WAXS results showed that CNCs were randomly distributed within the gel network in the unstretched state, exhibiting typical isotropic scattering characteristics (Fig. 1(g)). Under uniaxial stretching, CNCs underwent significant directional alignment along the principal strain direction, forming a highly ordered microstructure that induced pronounced optical anisotropy on the macroscopic scale. Furthermore, the calculated f increased from 0 to 0.90754 (Fig. S8 in the ESM). Based on this experimental evidence, we proposed the following structural evolution mechanism: In the initial state, the dynamic covalent bonds are in a stable associated state with CNCs dispersed within the three-dimensional network, potentially forming locally ordered regions, while the system overall exhibits isotropy. When the uniaxial tensile stress is applied, some boronic ester bonds break, and the gel network reconstitutes. The orientational relaxation time of the CNCs is much longer than the recombination time of the dynamic covalent bonds. Therefore, after stress removal, the dynamic network can complete bond reformation before the relaxation of the aligned CNCs structure, effectively "locking" the stretch-induced alignment of the CNCs within the gel network. Subsequently, under confined drying conditions (35% relative humidity, 25 °C), the removal of water molecules caused the polymer chains to contract, exerting a strong nanoconfinement effect on the CNCs that synergistically enhanced their degree of orientation, ultimately leading to a coordinated enhancement in both the birefringence and the order of interference colors.

Given that the alignment of CNCs predominantly governs the orientational changes within the dynamically cross-linked hydrogel, this system serves as an ideal platform for investigating the alignment behavior of CNCs in a three-dimensional gel network. Therefore, this study employed a dynamic covalent hydrogel system to systematically investigate the influence mechanisms of various parameters on the alignment behavior of CNCs.

3.1.2 *Buffer concentration*

The introduction of an effective buffer maintained a stable pH in the precursor system (Fig. 2(a)). The dynamic hydrogel utilizes phenylboronic acid/catechol complexes, formed from DMA and

PBAAM, as crosslinkers, whose complexation ability is highly dependent on the solution pH. Without buffer addition, the incorporation of crosslinkers caused the system pH to rapidly deviate from the optimal range, leading to incomplete or even failed complexation between phenylboronic acid and catechol [27], ultimately preventing gel formation (Fig. 2(b)).

The color development behavior of the hydrogel was closely related to the buffer concentration. When the concentration of the borax-NaOH buffer system was increased to 0.05 M, the sample exhibited a distinct transition in interference colors during the air-drying stage (Fig. 2(c) and Fig. S9 in the ESM). Observations under natural light revealed that as the buffer concentration increased from 0.0125 to 0.05 M, the selective precipitation of yellow-brown borax crystals gradually appeared in the dried gel films (Fig. S10 in the ESM). No significant crystallization was observed at the low concentration of 0.0125 M. At 0.025 M, the crystallization preferentially occurred in the central region of the hydrogel (the area of maximum CNCs orientation). Under the high-concentration condition of 0.05 M, crystal regions not only formed with significantly increased density in the highly oriented central area, but also gave rise to distinct crystal-enriched bands at the edges of the hydrogel (Fig. 2(d)). Experiments confirmed that increased buffer concentration induced crystal nucleation and growth by altering solute supersaturation. This phase separation process, through the induced light scattering and structural heterogeneity, ultimately significantly altered the birefringent color characteristics of the dynamic hydrogel.

The comparative analysis between polarized and natural light

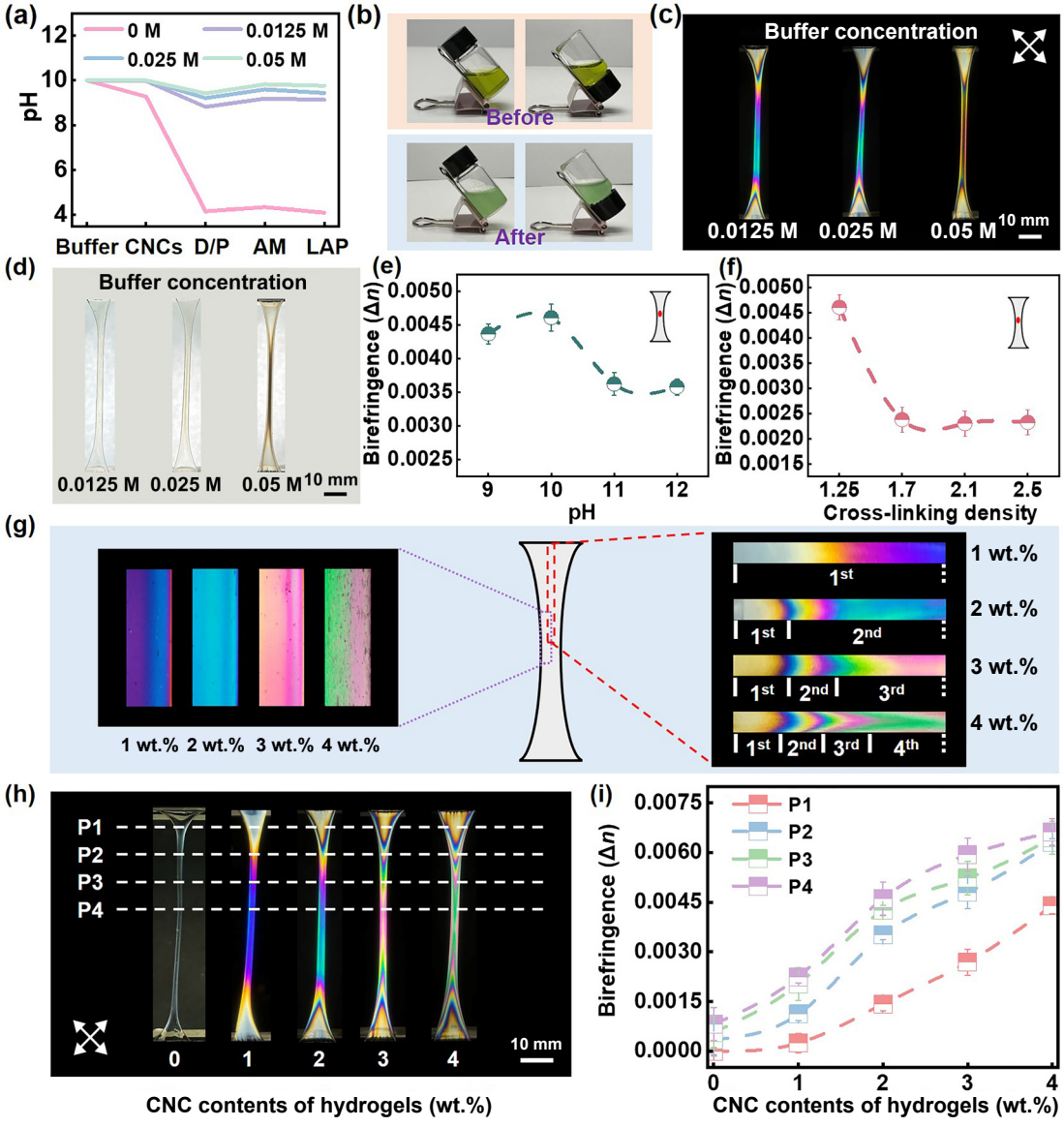

Figure 2 Regulatory mechanism of hydrogel precursor parameters on the optical performance of photonic gels. (a) pH variation trend of gel precursor solutions with different buffer concentrations. (b) Comparison of the macroscopic state of the precursor before and after UV polymerization under buffer-free conditions (anhydrous copper sulfate staining was used to enhance visualization). (c) Polarized optical images of photonic gel films with different buffer concentrations (λ = 6). (d) Macroscopic images of photonic gel films with different buffer concentrations (λ = 6). (e) Birefringence of photonic gel films at an elongation ratio of λ = 6 under different pH conditions. (f) Birefringence of photonic gel films at λ = 6 under different crosslinking densities. (g) POM images of photonic gel films prepared with different CNCs contents. (h) Polarized optical images of photonic gel films with different CNCs contents under stretching at λ = 6. (i) Effect of CNCs contents on the birefringence of photonic gel films at λ = 6.

imaging revealed the spatial selectivity of stretch-induced borax crystallization (Figs. S10 and S11 in the ESM). Notably, in blank systems with identical buffer concentration but without CNCs, the stretching and air-drying led to macroscopic phase separation characterized by disordered aggregation of borax molecules. In contrast, the CNCs-incorporated system exhibited remarkable spatial localization of crystals. Under the axial stress field, the CNCs aligned along the stretching direction, forming a gradient distribution from the central axis toward the edge regions. This anisotropic structure provided directed nucleation sites for borax crystals. This study demonstrates that the synergistic effect between intermolecular interactions at the CNCs–borax composite interface and the stress distribution within the polymer network ultimately promoted the oriented epitaxial growth of crystals in CNCs-enriched regions, resulting in an ordered crystalline structure with spatial selectivity.

3.1.3 *Precursor pH*

The precursor pH is a critical determinant of the coordination efficiency and stability between the cross-linker, phenylboronic acid, and catechol. Therefore, we systematically investigated the effect of buffer pH (9–12) on the structural-optical properties of dynamic hybrid hydrogels (buffer concentration of 0.0125 M, crosslinking density x = 1.25, CNCs concentration of 2 wt.%, and λ = 6). We found that intact three-dimensional networks formed under all pH conditions, indicating excellent chemical stability of the system across a broad alkaline range (Fig. S12 in the ESM). Under similar film thickness conditions, samples at pH = 10 exhibited the maximum optical retardation, closely associated with the internally formed ordered orientation structure. Birefringence calculations further confirmed that the optimal alignment degree corresponded to pH = 10 (Fig. 2(e)). Conversely, at pH = 12, the tensile stress no longer decreased with strain but increased substantially. The greatly increased rigidity of the crosslinked network severely restricted the CNCs alignment, leading to reduced optical retardation (Fig. S13 in the ESM) [28].

3.1.4 *Crosslinking density*

The investigation into the regulation of structural-optical properties by crosslinking density (x = 0.8–2.5) in CNCs-composite hydrogels showed that excessively low crosslinking density (x = 0.8) prevented the formation of a continuous polymer network, resulting in a sol state (Fig. S14 in the ESM). As the crosslinking density increased, the interference fringe order in the photonic gel films decreased, indicating that high crosslinking density suppressed the chain segment mobility and cooperative orientation of CNCs/polymers [29]. Concurrently, the elastic modulus of the hydrogels increased with crosslinking density (Fig. S15 in the ESM), as the tighter network restricted the free movement of molecular chains. Birefringence calculations confirmed that the optimal orientation alignment corresponded to a crosslinking density of x = 1.25 (Fig. 2(f)).

3.1.5 *CNCs contents of hydrogels*

The CNCs content demonstrated high tunability over the birefringent colors of the photonic gel films. Current study showed that even minor variations in CNCs content (1 wt.%–4 wt.%) resulted in significant changes in birefringent colors (Fig. S16 in the ESM). Systematic analysis of radial POM images revealed a clear hierarchical correspondence between the interference color order and CNC concentration: As the content increased from 1 wt.% to 4 wt.%, the interference order progressively increased from 1st to 4th order (Fig. 2(g)). This phenomenon indicates that the introduction of CNCs effectively promoted internal structural ordering, thereby enhancing the optical anisotropic response. Furthermore, with increasing the content of CNCs, their role as rigid nano-reinforcing phases became more pronounced, collectively enhancing the elastic modulus and mechanical strength of the composites (Fig. S17 in the ESM). However, the high-resolution polarized optical microscopy further revealed characteristic patterns of structural defect evolution associated with CNCs addition. The magnified microscopic analysis demonstrated that large particles induced aberrations in color transition zones and structural imperfections. With increasing CNCs content, the density of large particles in the photonic gel films rose significantly, accompanied by markedly aggravated microscopic defects. This phenomenon was directly correlated with the CNCs aggregation behavior, as evidenced by macroscopic photographs showing decreased transparency and disappearance of the Tyndall effect (Fig. S18(a) in the ESM); reduced zeta potential indicating diminished colloidal stability (Fig. S18(b) in the ESM); and increased average particle size with altered size distribution directly reflecting enhanced aggregation (Figs. S18(c)–S18(f) in the ESM). This aggregation phenomenon originates from the enhanced inter-CNCs interactions at elevated concentrations, which consequently increase the aggregation propensity, thereby compromising both the color uniformity and transition smoothness of the films.

We further investigated quantitative analysis of birefringence measured at different spatial positions (P1–P4). Results indicated that the pure polyacrylamide system without CNCs exhibited only weak optical anisotropy at an elongation ratio of λ = 6. Although the PAM network aligned slightly during confined drying, its contribution to the interference color signal was limited (Figs. 2(h) and 2(i)). The addition of CNCs significantly altered the anisotropy evolution path of the system. As the content increased from 1 wt.% to 4 wt.%, the birefringence at all characteristic positions showed a systematic enhancement trend (Δn = 0.00024–0.00662), indicating a significant improvement in the internal structural order with increasing CNCs content. The birefringence from positions P1 to P4 exhibited a clear spatial gradient, with Δn values in the central regions (corresponding to higher-numbered positions) being significantly higher than those at the ends. This phenomenon confirms the formation of a gradient orientation structure of CNCs along the stress direction during uniaxial stretching, with a higher degree of CNCs alignment in the central part of the material compared to the end regions, thereby establishing a spatial correlation from macroscopic deformation to microscopic alignment.

These results indicate that although increasing the CNCs content enhances the birefringence effect, excessively high concentrations will induce structural heterogeneity due to the agglomeration, compromising the optical quality and functionality of the material. Therefore, in practical applications, the CNCs concentration needs to be controlled within an appropriate range to achieve a balance between precise optical performance tuning and material structural integrity.

3.1.6 *Agglomeration of CNCs*

The dynamic covalent hydrogel system employed in this study exhibits significant pH dependence in its crosslinking reaction, necessitating the use of a suitable buffer solution to maintain the pH stability during the process. However, the introduced CNCs are

highly sensitive to salt components. The type and ionic strength of the buffer solution significantly regulate the colloidal stability and dispersion state of the CNCs by influencing the structure of their surface electrical double layer [30].

To systematically investigate this effect, three buffer systems at pH = 10 were selected, including 0.0125 M borax-NaOH, 0.25 M sodium carbonate-sodium bicarbonate, and 0.5 M Tris-NaOH. CNC-composite dynamic hydrogels were prepared in each system through ultrasonic treatment (580 W, 37 kHz, 30 min) (Fig. 3(a)(i)). Experimental results demonstrated that different buffer systems induced markedly different states of the CNCs agglomeration (Figs. 3(a)(ii) and 3(a)(iii), and Fig. S19 in the ESM). The borax-NaOH system yielded the optimal dispersion stability for CNCs, primarily attributed to its suitable ionic strength and alkaline environment, which effectively maintained the electrostatic stabilization mechanism provided by the negative surface charges on the CNCs [31]. This disparity in dispersibility directly influenced the macroscopic optical properties of the hydrogels (Fig. 3(b)). The highly dispersed state of CNCs in the borax system significantly reduced light scattering centers, thereby enhancing the transmittance of the material (Fig. 3(c)). Furthermore, it was confirmed that the ultrasonic treatment effectively disrupted initial CNCs agglomerates, significantly improving the material transparency [32]. Concurrently, as water evaporated from the gel, the contraction and densification of the polymer network further reduced internal light-scattering interfaces, also contributing to an overall increase in material transmittance (Fig. S20 in the ESM).

Despite the different buffer types, all hydrogels exhibited an evolution of birefringence colors, transitioning from local to long-range order with increasing elongation ratio (λ). This indicates that the uniaxial stretching effectively induces global ordering of the microstructure, i.e., promoting the consistent alignment of cellulose nanocrystals along the stretching direction. This phenomenon remained consistent across different buffer systems, demonstrating that the mechanism of stretch-induced consistent CNCs alignment along the stress direction is universal and not contingent on the specific chemical environment (Fig. 3(e)).

The quantitative analysis of Δn for different samples further revealed the intrinsic relationship between the dispersion state of CNCs and the resulting optical performance (Fig. 3(d)). The results showed a clear gradient distribution of Δn, which exhibited a significant positive correlation with the initial dispersion state of the CNCs in the precursor solution. Notably, the borax-NaOH buffer system subjected to 30-min ultrasonic treatment represents the optimal condition for CNCs dispersion. This created favorable conditions for achieving a highly ordered arrangement within the three-dimensional network, ultimately enabling the material to exhibit superior optical anisotropic properties.

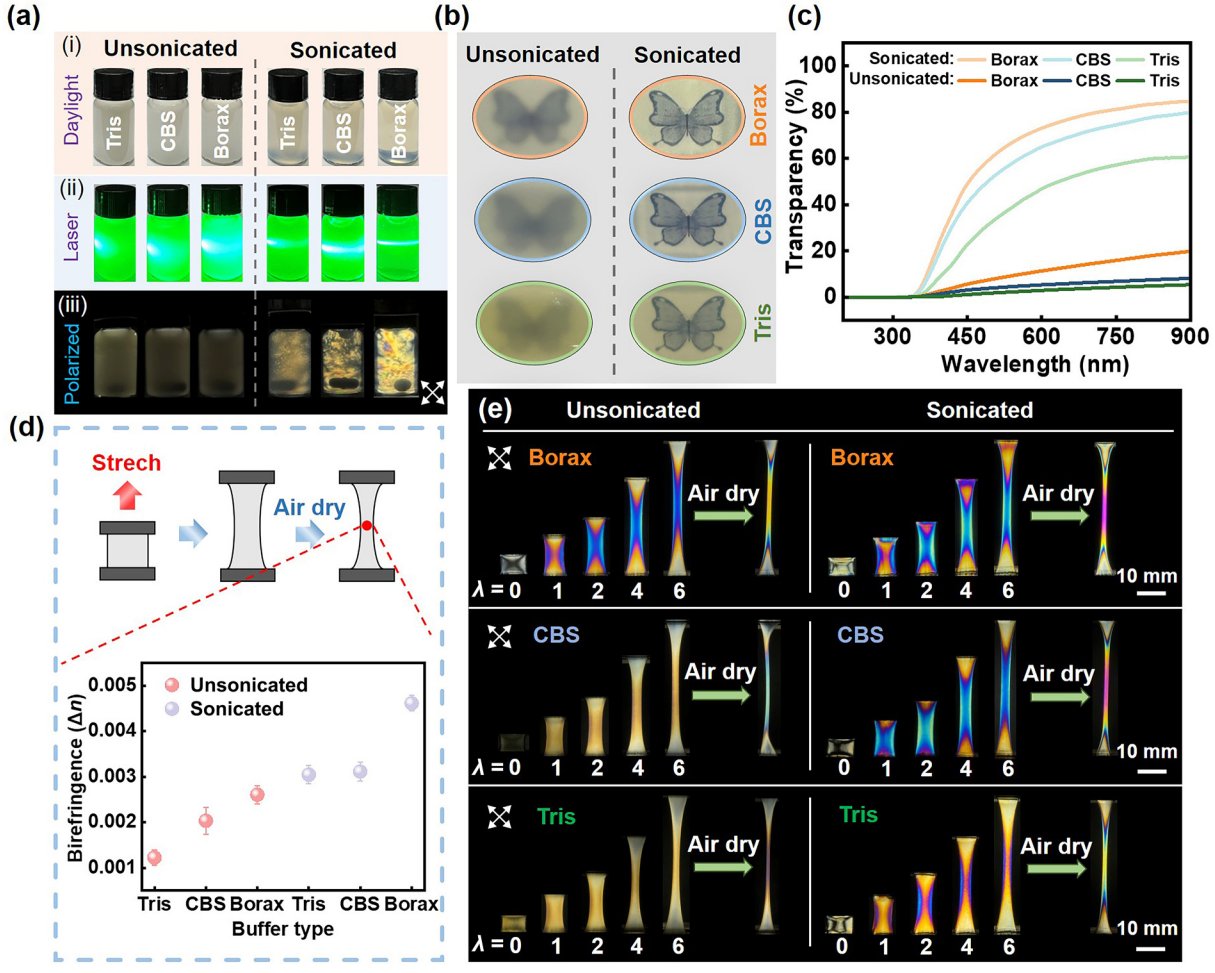

Figure 3 Effects of the aggregation degree on the optical performance of photonic gel materials. (a) Macroscopic image of the precursor. (i) Macroscopic state of the precursors, (ii) laser scattering behavior of the colloidal systems, and (iii) birefringence observation of the precursors under polarized light. (b) Macroscopic morphology of the formed hydrogels. (c) UV–Vis absorption spectra. (d) Birefringence of the photonic gel films. (e) Polarized optical images under stretching.

The aforementioned phenomena confirm that the dispersion state of CNCs is a critical factor determining the final optical performance of the photonic gel. Their spatial distribution and alignment capability within the cured gel network are directly constrained by their initial dispersion quality in the precursor solution. If severe agglomeration of CNCs occurs in the precursor, their orientational capability as structural units during subsequent stretching will be significantly limited, leading to reduced overall alignment order and consequently diminishing the tunability of the material's optical anisotropy. Conversely, improving the dispersion of CNCs in the precursor via ultrasonic treatment effectively promotes their orderly rearrangement under stress, thereby broadening the optical response range of the photonic material.

In summary, under fixed stretching and geometric parameters, this study established the optimal preparation protocol for photonic gel film materials through systematic optimization of precursor parameters. The optimized parameters include: 0.0125 M borax-NaOH buffer (pH = 10), crosslinking density x = 1.25, CNCs content of 2 wt.%, combined with an ultrasonic treatment process. Under these conditions, the resulting material achieved a birefringence of 0.00461 and f of 0.90754, demonstrating excellent optical performance. Current work identified that the agglomeration behavior of CNCs in the precursor is the key factor influencing the final optical properties of the material, with the buffer salt concentration playing a decisive role in the agglomeration state. Therefore, precise control of the salt addition amount during preparation is crucial for obtaining high-performance photonic gel films.

3.2 Stretching conditions

Through systematic optimization of the key preparation parameters for the dynamic hybrid hydrogels, this study successfully fabricated photonic gel film materials with broad-range optical tunability. Furthermore, controlling the stretching parameters of the hydrogel is an effective approach for precisely regulating its birefringence characteristics.

3.2.1 *Elongation ratios*

The analysis of photonic gel film samples after air-drying under different elongation ratios (λ) revealed that the optical response of the dynamic hybrid hydrogel exhibits a significant λ-dependence. As λ increased, the interference color order of the dried samples showed a non-monotonic trend, initially strengthening and then weakening (Fig. 4(a)). Further quantitative analysis indicated that Δn of the material continuously increased with rising λ (Fig. 4(b)), directly confirming the progressive improvement in the degree of CNC alignment along the stretching direction. This phenomenon primarily stems from two synergistic physical mechanisms. On the one hand, as λ increases, the sample thickness correspondingly decreases, and birefringence is inversely related to sample thickness. On the other hand, the width contraction ratio of thesamples significantly increased with higher λ (Fig. 4(c)). This enhanced lateral contraction, through a strong spatial confinement effect, further promoted the directional alignment of CNCs within the gel matrix. Experimental data confirmed that this dynamic strain-induced confined alignment process effectively establishes a clear structure–property relationship between the elongation ratio and the orientational order of the CNCs.

Furthermore, although the birefringence increased continuously with λ, the optical retardation of the material exhibited a gradual decreasing trend due to the substantial reduction in sample thickness. This phenomenon reveals the distinct contribution mechanisms of geometric dimensional changes and intrinsic structural ordering to the optical performance during stretching: The increase in birefringence benefits from the enhanced degree of CNCs orientation, whereas the decrease in retardation is attributed to the shortened optical path length. Together, these factors determine the final interference color order exhibited by the material, explaining the non-monotonic trend observed in Fig. 4(a).

3.2.2 *Stretch speed*

This study showed that the stretching rate significantly influences the deformation behavior and optical response of the dynamic hydrogel. As the stretching rate increased, the Poisson's ratio of the hydrogel correspondingly increased, leading to more pronounced lateral contraction in samples subjected to high-speed stretching, while the thickness contraction was relatively smaller. This asymmetric deformation behavior induced changes in the optical path length. Specifically, the large width contraction induced by high stretching rates resulted in increased sample thickness, thereby increasing the optical retardation and ultimately causing an increase in the interference order (Fig. 4(d)).

Through systematic analysis of the sample birefringence, current study further revealed the regulatory effect of stretching rate on the anisotropic structure of the photonic gel films (Fig. 4(e)). Interestingly, the birefringence of the photonic gel films decreased with increasing stretching rate. This seemingly paradoxical phenomenon originates from a competition mechanism between the orientation kinetics of the CNCs and the network reconfiguration kinetics. During the high-speed stretching-stop process, the orientational rearrangement of the CNCs was not fully completed before its relaxation process was "frozen" by the rapidly reconfiguring dynamic covalent network. In contrast, a lower stretching rate provided sufficient response time for the CNCs, enabling them to achieve a more complete orientational alignment. However, excessively slow stretching rates significantly reduced production efficiency. Based on this analysis, this study identified 2.5 mm/min as the optimized stretching rate for achieving the best CNCs orientation.

3.3 Geometric dimensions

3.3.1 *Width*

Through precise design of the initial geometry of the dynamic hydrogels, their contraction behavior and the internal CNCs orientation distribution can be effectively regulated, thereby enabling accurate programming of the spatial optical properties of the resulting photonic gel films. We systematically fabricated hydrogel samples with uniform initial height (4 mm) and initial thickness (2 mm), while maintaining gradient variations in initial width (4–28 mm). Under a fixed elongation ratio (λ = 6), all samples were successfully transformed into photonic gel films exhibiting distinct structural colors (Fig. 5(a)).

Results revealed that the lateral contraction ratio of the photonic gel films decreased with increasing initial width (Fig. 5(c)). Significantly, the difference in birefringence between the central and edge regions of the samples became progressively more pronounced with higher initial width (W_0) values (Fig. 5(d)). This phenomenon can be attributed to the weakening geometric confinement effect: A larger initial width resulted in relatively weaker spatial constraints on the central region of the hydrogel during drying, thereby compromising the consistency of CNCs orientation in this area.

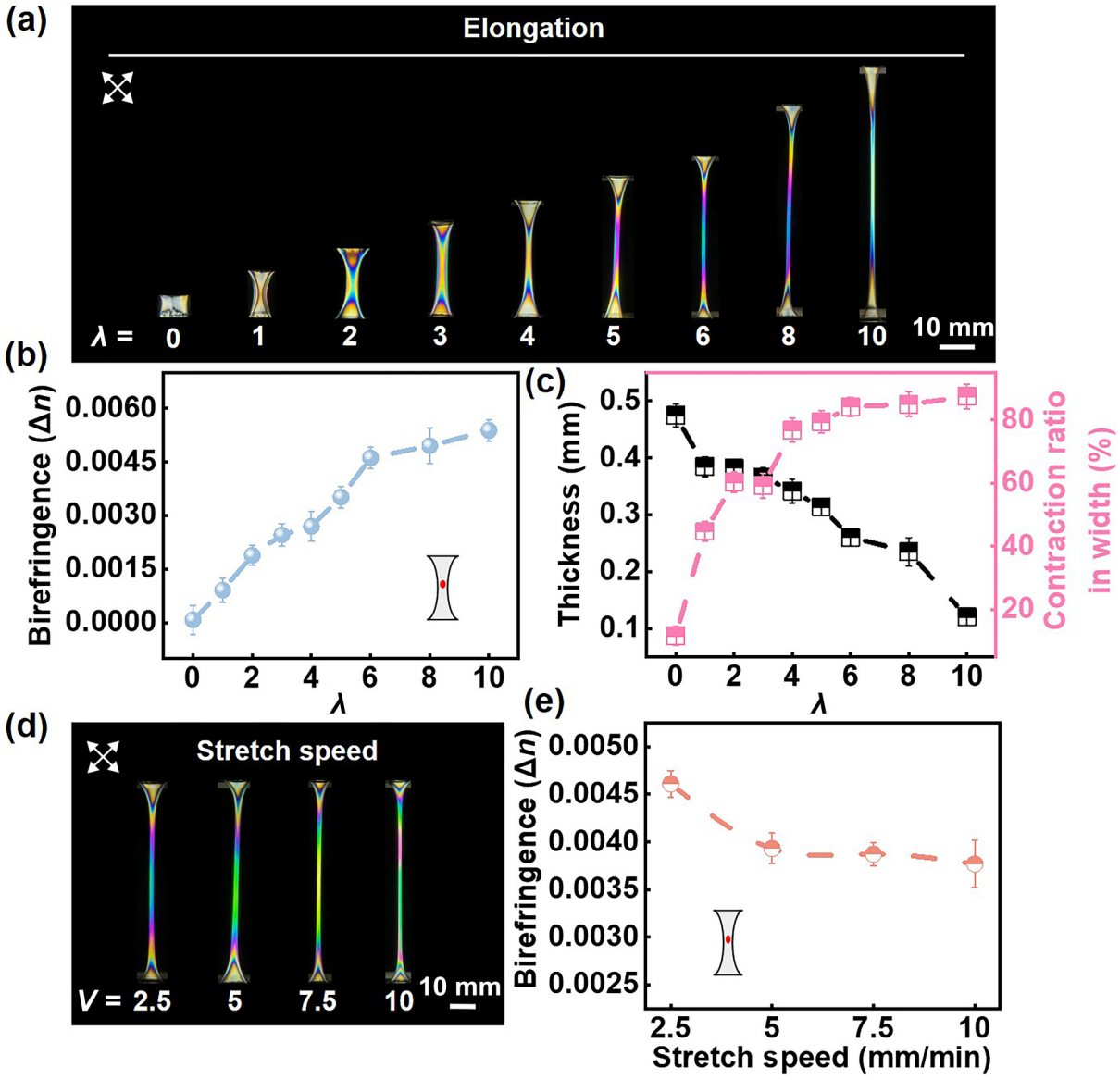

Figure 4 Governing principles of stretching parameters on the structure and properties of photonic gel films. (a) Polarized optical images showing the structural ordering induced by different elongation ratios (λ). (b) Quantitative evolution of birefringence with elongation ratio, reflecting the internal degree of orientation. (c) Variation of geometrical deformation (thickness and width contraction ratios) of the films as a function of elongation ratio. (d) Polarized optical images corresponding to different stretching rates at a constant elongation ratio (λ = 6), revealing the orientation kinetics. (e) Relationship between birefringence and stretching rate at λ = 6, quantitatively characterizing the dependence of the orientation process on the deformation rate.

Under the limiting condition of W_0 = 4 mm, the resulting photonic gel film exhibited highly coordinated contraction behavior in both width and depth directions (contraction ratios both approximately 85.7%). This isotropic, strong contraction not only promoted consistent CNCs orientation between the center and edge regions, achieving a maximum birefringence of 0.00497 ± 0.00022, but also minimized the transverse birefringence difference, demonstrating excellent optical homogeneity.

In contrast, when W_0 = 28 mm, the system exhibited significantly anisotropic contraction behavior: The width contraction ratio was only 29.2%, while the depth contraction ratio reached 97.2%. This asymmetric contraction induced a gradient CNCs orientation structure within the wide film, particularly generating a birefringence distribution ranging from 0.00202 to 0.00314 in the edge regions (Fig. 5(b)). Concurrently, a large-area uniform region with low birefringence (0.00089 ± 0.00012) formed in the middle of the film, presenting as a clearly separable uniform membrane.

3.3.2 *Thickness*

We further revealed a negative correlation between the initial thickness of the material and Δn. Experimental results demonstrated that as the initial hydrogel thickness increased, the extended optical path length within the material led to an increase in the accumulated phase retardation, macroscopically manifested as an enhancement in the interference order (Fig. 5(e)). However, higher thickness simultaneously suppressed the effective alignment of CNCs during stretching, causing a significant decrease in birefringence from 0.00487 to 0.00364 (Fig. 5(f)). This seemingly paradoxical phenomenon reveals the dual nature of the thickness

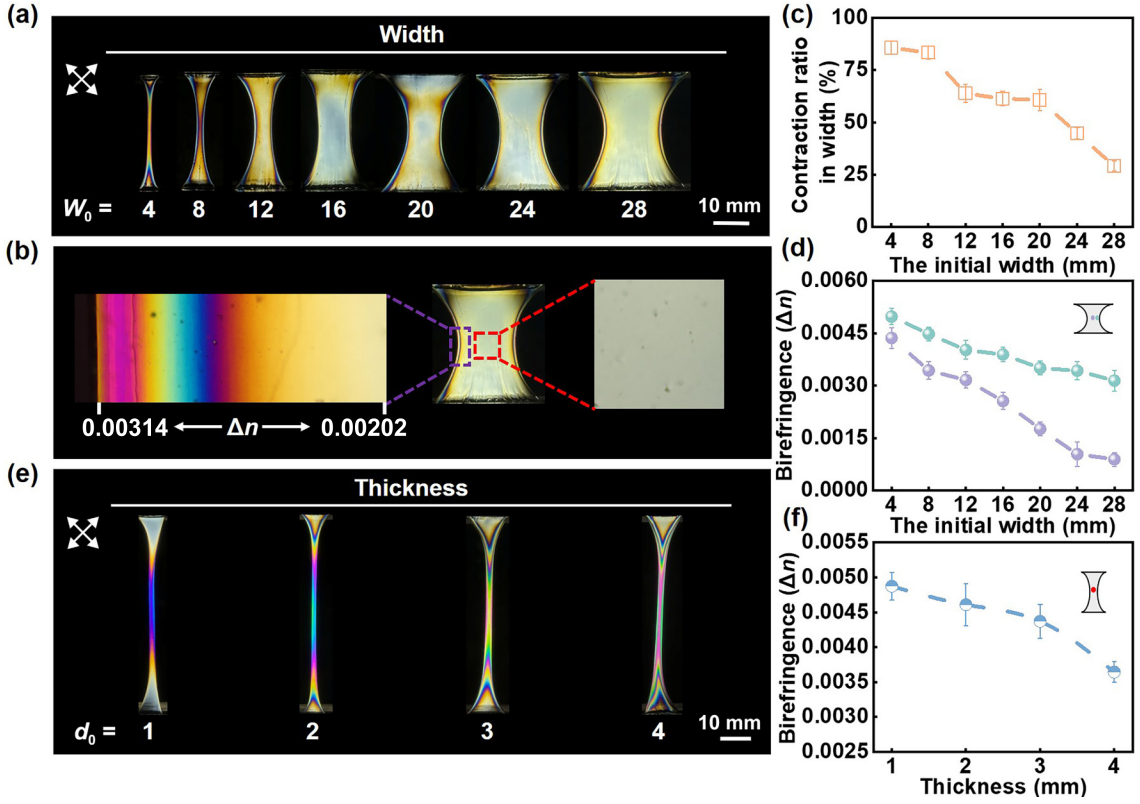

Figure 5 Governing principles of initial geometry on the structure and properties of photonic gel films. (a) Polarized optical images of photonic gel films with different W_0 at an elongation ratio of $\lambda = 6$. (b) Gradient birefringence distribution in the edge region and uniform birefringence in the central area of a sample with $W_0 = 28$ mm. (c) Width contraction ratios of photonic gel films with varying initial widths. (d) Birefringence values measured at the middle (purple) and edge (green) of position P4 in photonic gel films with different initial widths. (e) Polarized optical images of photonic gel films with different initial thicknesses (d_0) at $\lambda = 6$. (f) Birefringence of photonic gel films with different initial thicknesses at $\lambda = 6$.

effect: Although the prolonged optical path enhances the apparent interference phenomenon, the degree of orientational order of the CNCs within the material actually decreases markedly with increasing thickness.

By systematically deciphering the regulatory principles of hydrogel geometry on CNCs alignment and optical performance, this study establishes a quantitative relationship from initial geometric parameters to final optical characteristics. This provides an important theoretical basis and process guidance for designing photonic gel films with spatially programmable optical properties.

3.4 Efficient utilization

Experimental results indicated that region P4 of the xerogel exhibited the highest values of optical retardation and birefringence. Based on this finding, this study precisely excised this optically optimal region (Fig. 6(a)) and employed a multi-layer stacking strategy (Fig. 6(b)), a method previously established where the total optical retardation of a stacked film assembly equals the sum of the retardations of the individual layers [33]. Rational stacking effectively prolongs the optical path, thereby enhancing the overall optical retardation effect of the structure. Consequently, by precisely controlling the optical retardation characteristics of individual films, the broadest interference color gamut coverage can be achieved with the minimal number of stacked layers.

The most effective parameter systems for regulating the alignment degree of CNCs are the CNCs loading content and the ultrasonic dispersion process. Results demonstrated that prior to systematic parameter optimization, achieving the broadest interference color gamut required a CNCs loading of 0.85 wt.%. Furthermore, due to the absence of ultrasonic treatment, CNCs exhibited significant agglomeration, with numerous macroscopic particles visible within the material (Fig. 6(c)). In contrast, following the systematic optimization of the preparation parameters, the required CNCs loading for superior optical performance was reduced to 0.375 wt.%. The number of macroscopic particles in the samples decreased markedly, indicating a significant improvement in the dispersion uniformity of CNCs within the photonic gel films, which subsequently led to a comprehensive enhancement of optical properties (Fig. 6(d)). This optimization strategy achieved an approximately 55.9% reduction in CNCs consumption, not only substantially lowering raw material costs but also highlighting the significant advantage of our preparation strategy in terms of resource utilization efficiency. Through systematic parameter optimization and leveraging existing stacking techniques, this study significantly reduces the required amount of CNCs, providing an important technical pathway for developing high-performance, low-cost, and sustainable photonic devices.

4 Conclusions

In this study we systematically investigated the alignment behavior and underlying regulatory mechanisms of CNCs composite hydrogels with different crosslinking types (irreversible versus reversible) under uniaxial stretching. Through an in-depth analysis of the reversible nature of the hydrogel network, we elucidated its critical role in achieving highly ordered alignment of CNCs. Specifically, the study revealed that, in contrast to irreversibly cross-

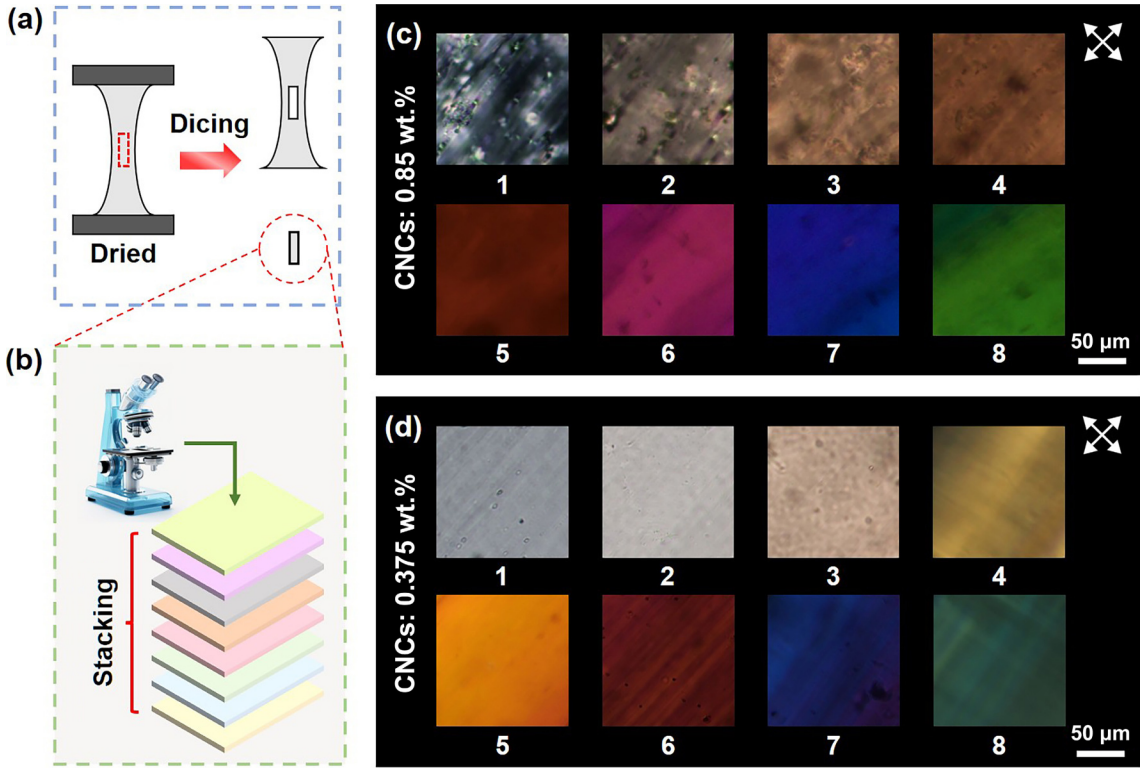

Figure 6 (a) Schematic diagram illustrating the fabrication process of the photonic gel material. (b) Schematic of the layered stacking configuration. (c) Minimum CNCs loading (0.85 wt.%) required to achieve the target optical performance without parameter optimization. (d) Minimum CNCs loading (0.375 wt.%) required to achieve the target optical performance after systematic optimization, demonstrating a significant enhancement in resource efficiency.

linked networks, the unique dynamic bond exchange behavior in reversibly cross-linked networks under stretching allows the gel to effectively transmit tensile stress while maintaining sufficient reconfigurability. This dual functionality actively facilitates the rearrangement and alignment of CNCs. Consequently, these insights enabled the fabrication of homogeneous photonic gel materials that exhibit outstanding optical performance alongside a 55.9% reduction in CNCs loading. Overall, this work provides an effective strategy to overcome the limitations of traditional CNCs alignment techniques, while enhances the understanding of the structural evolution principles of nanomaterials within gel matrices for developing advanced energy-efficient smart cellulose-based photonic materials.

Electronic Supplementary Material: Supplementary material (^{1}H NMR spectra, TEM characterization data, stress–strain measurements, orientation index calculations, dynamic light scattering analysis, polarized optical images, and zeta potential measurements) is available in the online version of this article at https://doi.org/10.26599/NR.2026.94908338.

Data availability

All data needed to support the conclusions in the paper are presented in the manuscript and the Electronic Supplementary Material. Additional data related to this paper may be requested from the corresponding author upon request.

Acknowledgements

P. W. L. acknowledges the start-up funding from Huazhong Agricultural University (No. 11042110020) and the Hubei Key R&D Program (No. 2024BBB077). L. G. P. acknowledges the support from the Hunan Provincial Natural Science Foundation of China (No. 2024JJ9491), the Changsha Municipal Health Commission (No. KJ-A2023003), and the Changsha Science and Technology Program (No. kq2403170).

Declaration of competing interest

All the contributing authors report no conflict of interest in this work.

Author contribution statement

Y. W. R.: Data curation, project administration, validation, writing manuscript, experimental design. L. N. M.: Data curation, project administration, validation, experimental design. Q. W. L.: Project administration. A. R. A.: Writing – review & editing. T. W. L.: Validation. Q. S.: Project administration. L. G. P.: Project administration. S. P. Y.: Project administration. J. L.: Project administration. D. D. Y.: Project administration. P. W. L.: Project administration, funding acquisition, writing – review & editing. All the authors have approved the final manuscript.

Use of AI statement

None.

References

[1] Duan, C. L.; Cheng, Z.; Wang, B.; Zeng, J. S.; Xu, J.; Li, J. P.; Gao, W. H.; Chen, K. F. Chiral photonic liquid crystal films derived from cellulose nanocrystals. *Small* **2021**, *17*, 2007306.

[2] Khan, M. N.; Ahmad, A.; Rehman, N.; Kelestemur, S.; Tariq, M.; Jan, A. K.; Ahmad, S.; Eisele, D. M.; Syed, W.; Al-Rawi, M. B. A. Extraction and characterization of cellulose and cellulose nanocrystals from the stalks of *Marrubium vulgare* plant. *Carbohydr. Polym. Technol. Appl.* **2025**, *11*, 100947.
[3] Hou, Y. L.; Zhang, Z.; Harrisson, S.; Sèbe, G. SI-ATRP grafting of polymers from polydopamine-modified cellulose nanocrystals. *Carbohydr. Polym.* **2024**, *341*, 122346.
[4] Sun, W.; Wang, J.; He, M. Anisotropic cellulose nanocrystal composite hydrogel for multiple responses and information encryption. *Carbohydr. Polym.* **2023**, *303*, 120446.
[5] Song, J. N.; Parker, R. M.; Frka-Petesic, B.; Deng, T.; Xu, L. Q.; Deng, X.; Vignolini, S.; Shen, Q. C. Spray-assisted fabrication of cellulose photonic pigments on superhydrophobic surfaces. *Adv. Mater.* **2025**, *37*, 2416607.
[6] Kelly, J. A.; Shukaliak, A. M.; Cheung, C. C. Y.; Shopsowitz, K. E.; Hamad, W. Y.; MacLachlan, M. J. Responsive photonic hydrogels based on nanocrystalline cellulose. *Angew. Chem., Int. Ed.* **2013**, *52*, 8912–8916.
[7] Zhang, F. S.; Li, Q. Y.; Wang, C. L.; Wang, D. D.; Song, M. Y.; Li, Z.; Xue, X. Y.; Zhang, G.; Qing, G. Multimodal, convertible, and chiral optical films for anti-counterfeiting labels. *Adv. Funct. Mater.* **2022**, *32*, 2204487.
[8] Dumanli, A. G.; Kamita, G.; Landman, J.; van der Kooij, H.; Glover, B. J.; Baumberg, J. J.; Steiner, U.; Vignolini, S. Controlled, bio-inspired self-assembly of cellulose-based chiral reflectors. *Adv. Opt. Mater.* **2014**, *2*, 646–650.
[9] Liu, P. W.; Wang, J. X.; Qi, H. J.; Koddenberg, T.; Xu, D.; Liu, S. Y.; Zhang, K. Biomimetic confined self-assembly of chitin nanocrystals. *Nano Today* **2022**, *43*, 101420.
[10] Tran, A.; Boott, C. E.; MacLachlan, M. J. Understanding the self-assembly of cellulose nanocrystals-toward chiral photonic materials. *Adv. Mater.* **2020**, *32*, 1905876.
[11] Momeni, A.; Hamad, W. Y.; MacLachlan, M. J. Using rotation to organize cellulose nanocrystals inside a fiber. *Nanoscale* **2022**, *14*, 7613–7620.
[12] Frka-Petesic, B.; Parton, T. G.; Honorato-Rios, C.; Narkevicius, A.; Ballu, K.; Shen, Q. C.; Lu, Z. H.; Ogawa, Y.; Haataja, J. S.; Droguet, B. E. et al. Structural color from cellulose nanocrystals or chitin nanocrystals: Self-assembly, optics, and applications. *Chem. Rev.* **2023**, *123*, 12595–12756.
[13] Huang, H. Q.; Wang, X. J.; Yu, J. C.; Chen, Y.; Ji, H.; Zhang, Y. M.; Rehfeldt, F.; Wang, Y.; Zhang, K. Liquid-behaviors-assisted fabrication of multidimensional birefringent materials from dynamic hybrid hydrogels. *ACS Nano* **2019**, *13*, 3867–3874.
[14] Zhu, S. H.; Wang, S.; Huang, Y. F.; Tang, Q. Y.; Fu, T. Q.; Su, R. Y.; Fan, C. Y.; Xia, S.; Lee, P. S.; Lin, Y. H. Bioinspired structural hydrogels with highly ordered hierarchical orientations by flow-induced alignment of nanofibrils. *Nat. Commun.* **2024**, *15*, 118.
[15] Liu, J. J.; Yang, C. H.; Yin, T. H.; Wang, Z. J.; Qu, S. X.; Suo, Z. G. Polyacrylamide hydrogels. II. elastic dissipater. *J. Mech. Phys. Solids* **2019**, *133*, 103737.
[16] Xu, D.; Meng, X. T.; Liu, S. Y.; Poisson, J.; Vana, P.; Zhang, K. Dehydration regulates structural reorganization of dynamic hydrogels. *Nat. Commun.* **2024**, *15*, 6886.
[17] Agnelli, S.; Baldi, F.; Bignotti, F.; Salvadori, A.; Peroni, I. Fracture characterization of hyperelastic polyacrylamide hydrogels. *Eng. Fract. Mech.* **2018**, *203*, 54–65.
[18] Bertsch, P.; Isabettini, S.; Fischer, P. Ion-induced hydrogel formation and nematic ordering of nanocrystalline cellulose suspensions. *Biomacromolecules* **2017**, *18*, 4060–4066.
[19] Bertsch, P.; Sánchez-Ferrer, A.; Bagnani, M.; Isabettini, S.; Kohlbrecher, J.; Mezzenga, R.; Fischer, P. Ion-induced formation of nanocrystalline cellulose colloidal glasses containing nematic domains. *Langmuir* **2019**, *35*, 4117–4124.
[20] Hyon, S. H.; Cha, W. I.; Ikada, Y. Preparation of transparent poly(vinyl alcohol) hydrogel. *Polym. Bull.* **1989**, *22*, 119–122.
[21] Wan, B. L.; Liu, N. N.; Zhang, Z.; Fang, X.; Ding, Y. G.; Xiang, H. S.; He, Y. Q.; Liu, M. X.; Lin, X. M.; Tang, J. T. et al. Water-dispersible and stable polydopamine coated cellulose nanocrystal-MXene composites for high transparent, adhesive and conductive hydrogels. *Carbohydr. Polym.* **2023**, *314*, 120929.
[22] Vukusic, P.; Sambles, J. R. Photonic structures in biology. *Nature* **2003**, *424*, 852–855.
[23] Guo, S. J.; Zhu, S. L.; Qiao, Y.; Feng, S. H.; Yang, X.; Kang, B. B.; Yue, C. J.; Zhang, Y. J.; Li, Z. Z.; Ye, Y. N. et al. Ultra-low hysteresis under large deformation enabled by fast chains relaxation in highly competitive dynamic hydrogen bond networks. *Adv. Sci.* **2025**, *12*, e05417.
[24] Gong, X. H.; Luo, Y.; Zhang, C. Q.; Xie, J. T.; Wang, Y. Carboxymethyl chitosan-based tough hydrogels with low mechanical hysteresis and high conductivity as multifunctional sensors. *Chem. Eng. J.* **2025**, *510*, 161610.
[25] Zhao, J. M.; Meng, F. L. Modeling viscoelasticity and dynamic nematic order of exchangeable liquid crystal elastomers. *Phys. Rev. Lett.* **2023**, *131*, 068101.
[26] Kumar, A.; Rao, K. M.; Han, S. S. Mechanically viscoelastic nanoreinforced hybrid hydrogels composed of polyacrylamide, sodium carboxymethylcellulose, graphene oxide, and cellulose nanocrystals. *Carbohydr. Polym.* **2018**, *193*, 228–238.
[27] Narkar, A. R.; Barker, B.; Clisch, M.; Jiang, J. F.; Lee, B. P. pH responsive and oxidation resistant wet adhesive based on reversible catechol-boronate complexation. *Chem. Mater.* **2016**, *28*, 5432–5439.
[28] Wang, X. H.; Feng, N.; Shi, Z. X.; Zhou, N.; Lu, J.; Huang, J.; Gan, L. Stimuli-responsive flexible membrane via co-assembling sodium alginate into assembly membranes of rod-like cellulose nanocrystals with an achiral array. *Carbohydr. Polym.* **2021**, *262*, 117949.
[29] Lv, Z. K.; Zhao, H. H.; Li, Z. Y.; Qu, J. J.; Yang, S. K.; Liu, Y. F.; Zhang, W. B.; Zhang, L. Q.; Yue, T. K.; Liu, J. Unveiling nanoparticle diffusion mechanisms confined in different polymer topologies. *Macromolecules* **2025**, *58*, 11017–11028.
[30] Lu, S. Y.; Hu, X. N.; Xu, B.; Bai, C. Y.; Wang, T. H.; Ma, T.; Song, Y. Effects of different salt ions on the structure and rheological behavior of sulfated cellulose nanocrystal hydrogel. *Food Hydrocolloids* **2024**, *151*, 109799.
[31] Wang, S. H.; Yu, Z. Y.; Sun, X.; Panahi-Sarmad, M.; Yang, P.; Zhu, P. H.; Zhu, Y. L.; Liu, H.; Jiang, F. A universal strategy to mitigate microphase separation via cellulose nanocrystal hydration in fabricating strong, tough, and fatigue-resistant hydrogels. *Adv. Mater.* **2025**, *37*, 2416916.
[32] Nugroho, R. W. N.; Tardy, B. L.; Eldin, S. M.; Ilyas, R. A.; Mahardika, M.; Masruchin, N. Controlling the critical parameters of ultrasonication to affect the dispersion state, isolation, and chiral nematic assembly of cellulose nanocrystals. *Ultrason. Sonochem.* **2023**, *99*, 106581.
[33] Yang, Y.; Wang, X. J.; Huang, H. Q.; Cui, S. Q.; Chen, Y.; Wang, X. H.; Zhang, K. Modular nanocomposite films with tunable physical organization of cellulose nanocrystals for photonic encryption. *Adv. Opt. Mater.* **2020**, *8*, 2000547.